Fig. 2

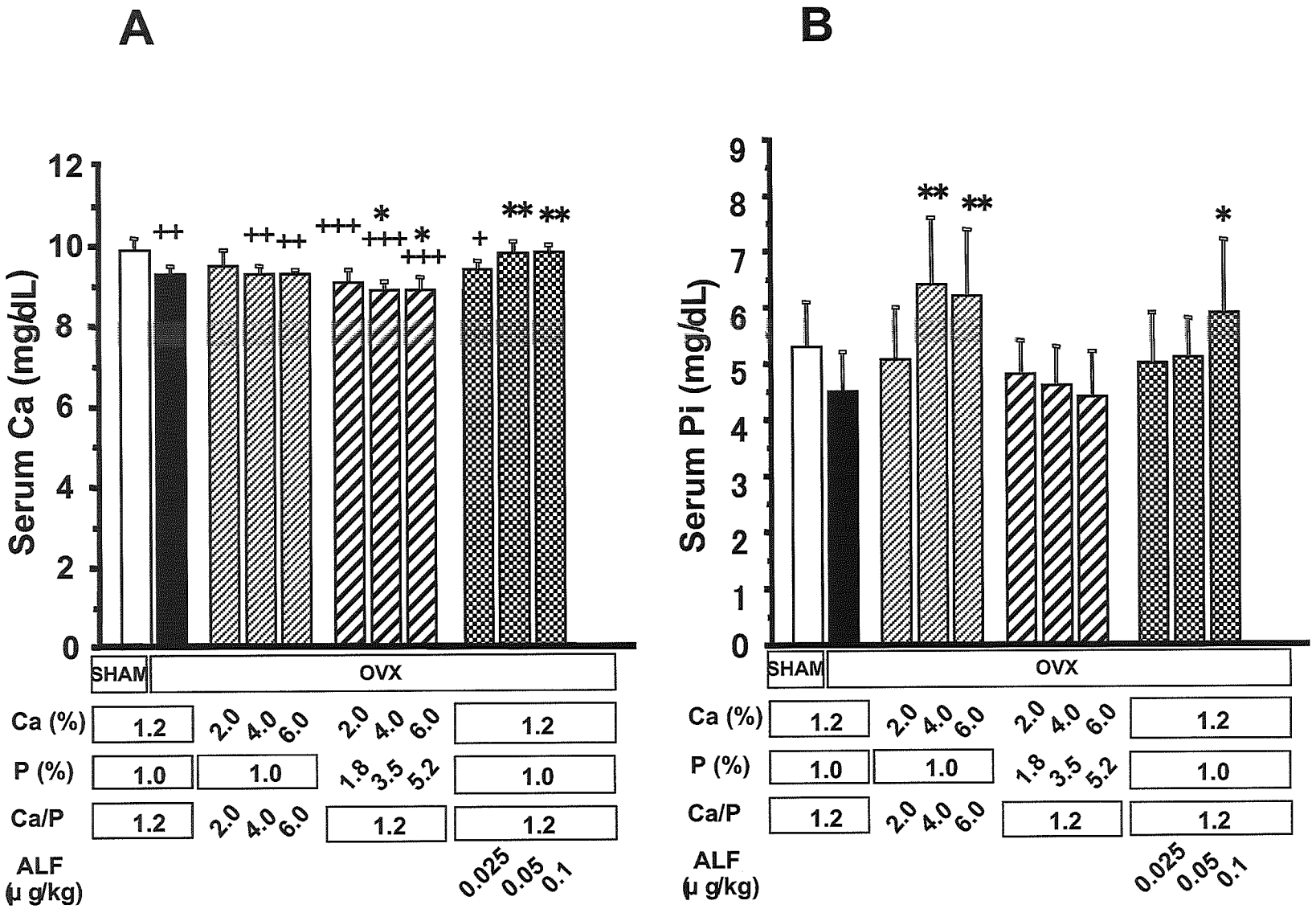
A
B
Serum Ca (mg/dL)
Serum Pi (mg/dL)
SHAM
OVX
Ca (%)
P (%)
Ca/P
ALF (μ g/kg)
1.2
1.0
2.0
4.0
6.0
1.8
3.5
5.2
0.025
0.05
0.1

Fig. 3

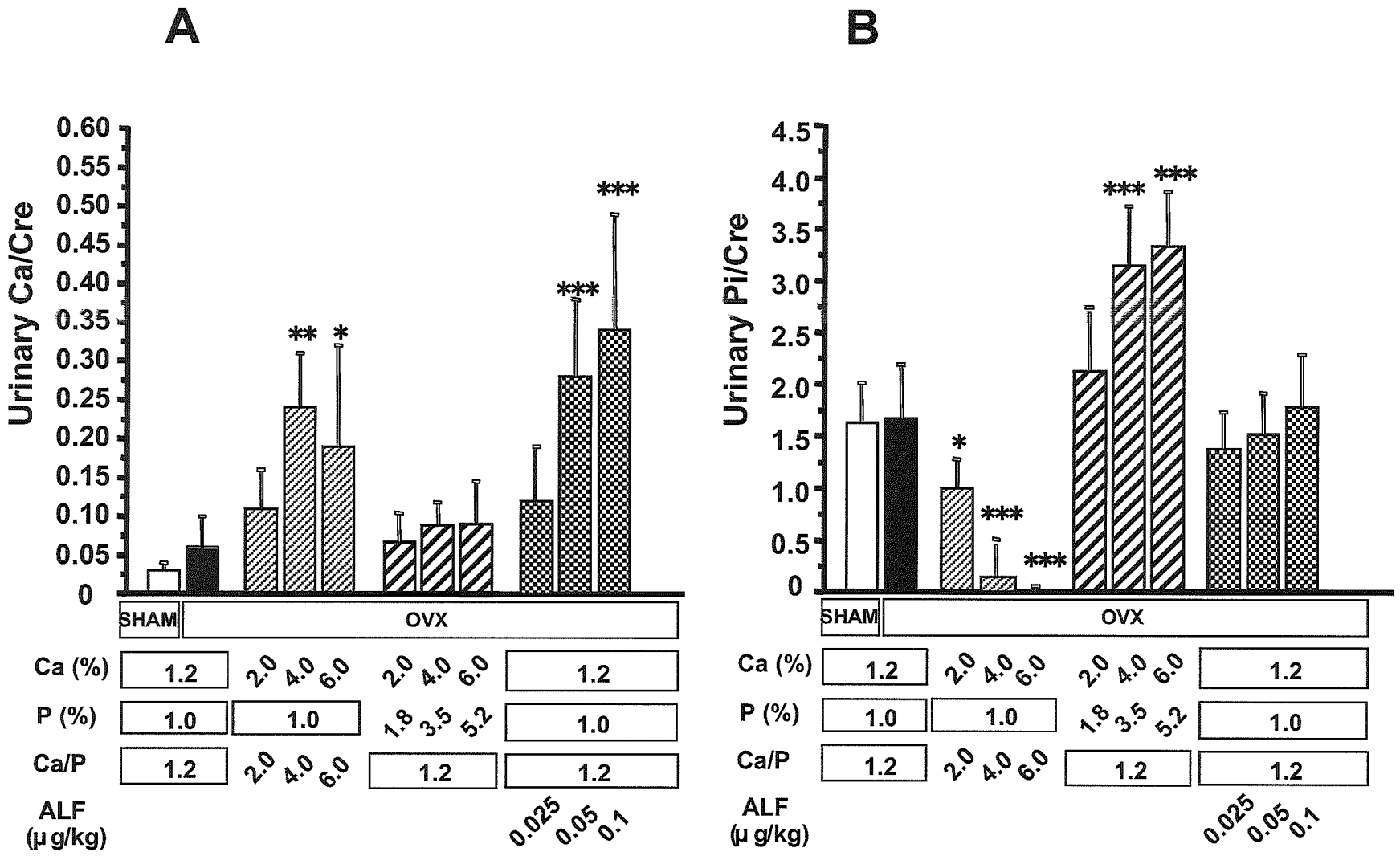
A
Urinary Ca/Cre
0.60
0.55
0.50
0.45
0.40
0.35
0.30
0.25
0.20
0.15
0.10
0.05
0
**
*
***
***
SHAM
OVX
Ca (%)
1.2
2.0
4.0
6.0
2.0
4.0
6.0
1.2
P (%)
1.0
1.0
1.8
3.5
5.2
1.0
Ca/P
1.2
2.0
4.0
6.0
1.2
1.2
ALF
(μg/kg)
0.025
0.05
0.1
B
Urinary Pi/Cre
4.5
4.0
3.5
3.0
2.5
2.0
1.5
1.0
0.5
0
*
***
***
***
***
SHAM
OVX
Ca (%)
1.2
2.0
4.0
6.0
2.0
4.0
6.0
1.2
P (%)
1.0
1.0
1.8
3.5
5.2
1.0
Ca/P
1.2
2.0
4.0
6.0
1.2
1.2
ALF
(μg/kg)
0.025
0.05
0.1

Fig. 4

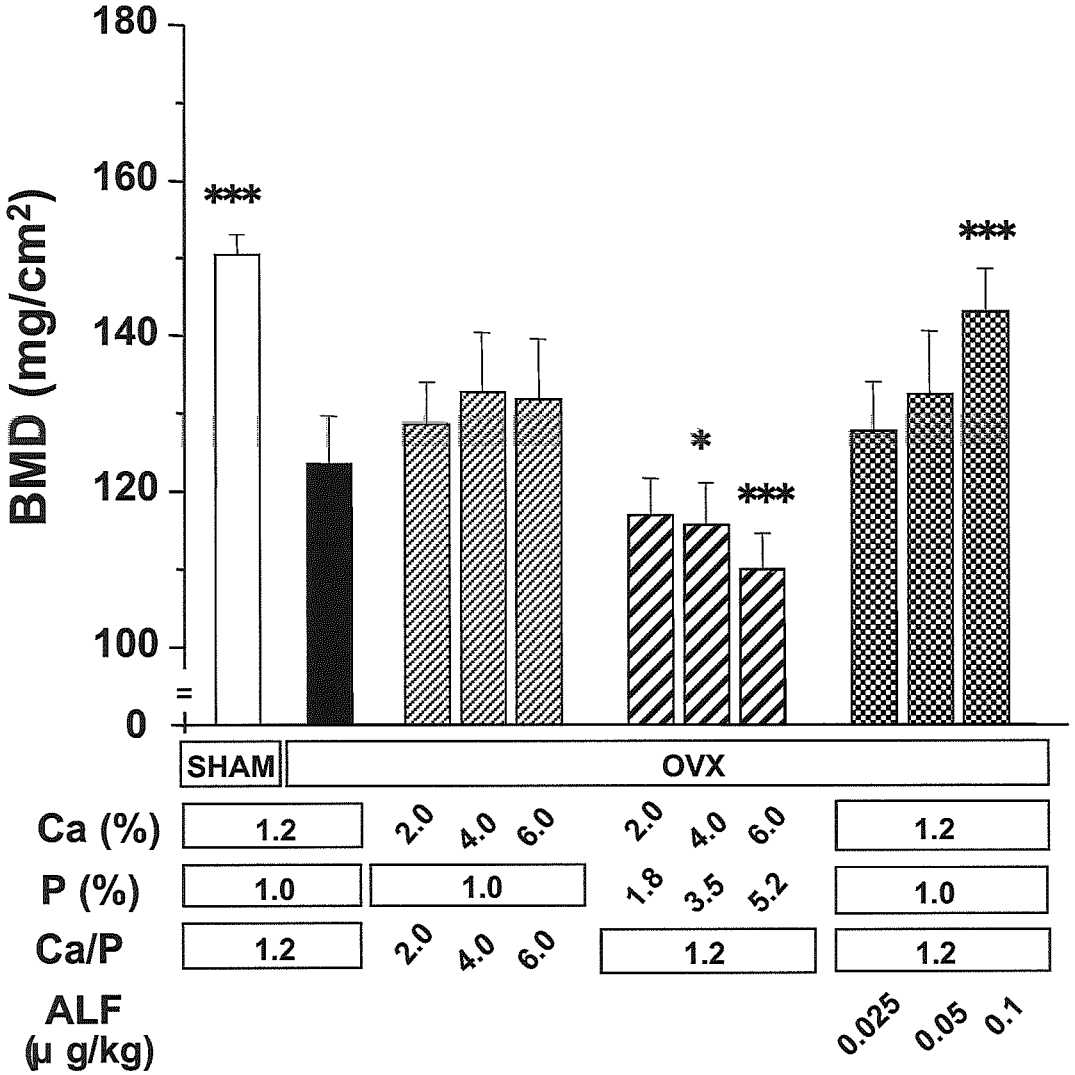
BMD (mg/cm²)
180
160
140
120
100
0
***
*
***
***
SHAM
OVX
Ca (%)
1.2
2.0
4.0
6.0
2.0
4.0
6.0
1.2
P (%)
1.0
1.0
1.8
3.5
5.2
1.0
Ca/P
1.2
2.0
4.0
6.0
1.2
1.2
ALF
(μ g/kg)
0.025
0.05
0.1

Fig. 5

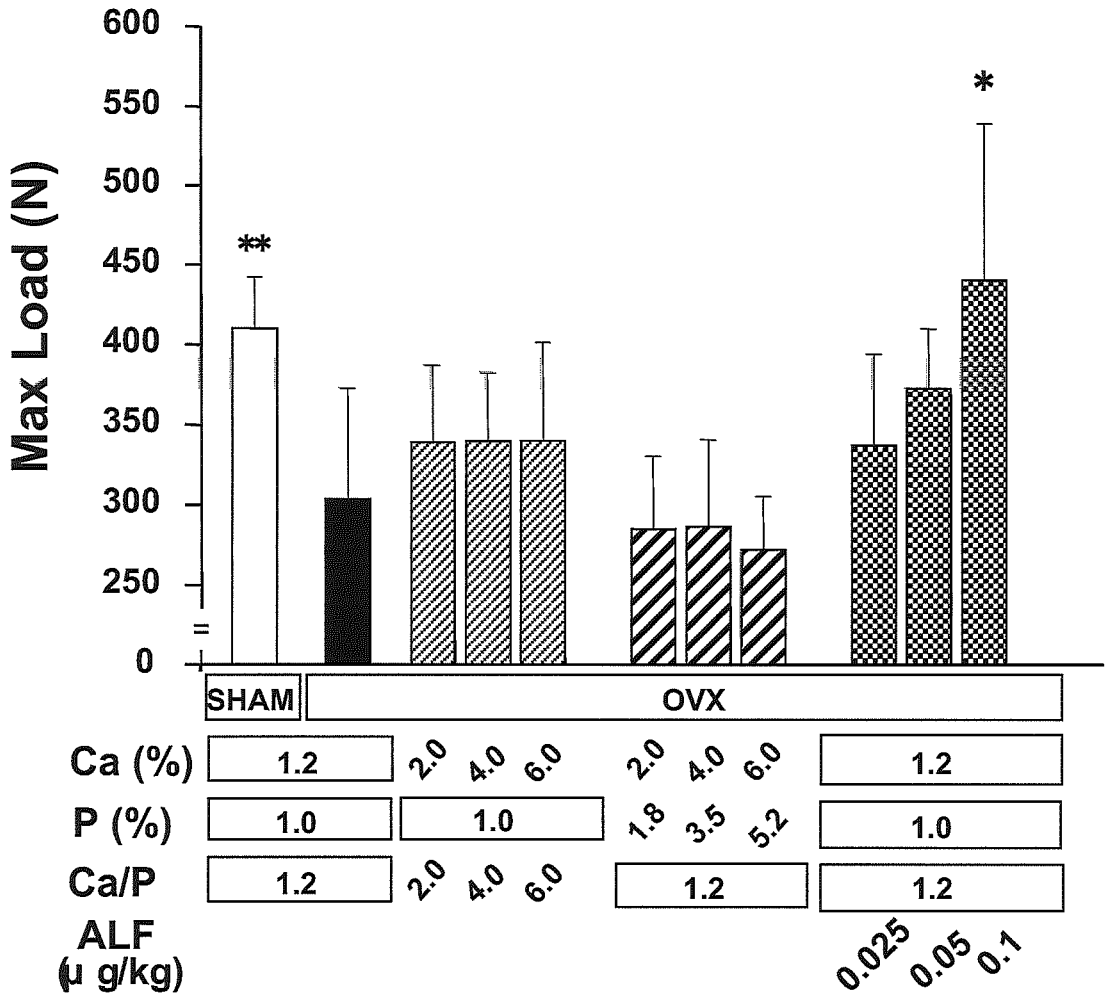
Max Load (N)
600
550
500
450
400
350
300
250
0
=
**
*
SHAM
OVX
Ca (%)
1.2
2.0
4.0
6.0
2.0
4.0
6.0
1.2
P (%)
1.0
1.0
1.8
3.5
5.2
1.0
Ca/P
1.2
2.0
4.0
6.0
1.2
1.2
ALF
(μ g/kg)
0.025
0.05
0.1

Table 2 Effects on architectural indices of lumbar vertebra

groups			structural indices		nonmetric indices	
operation	diet	agent	BV/TV (%)	Tb.N (/mm)	TBPf (/mm)	SMI
SHAM	A : Ca 1.2%, P 1.0%	vehicle	35.7± 2.3***	4.3 ± 0.1***	-3.15 ± 0.90***	43.4 ± 8.8***
OVX	A : Ca 1.2%, P 1.0%	vehicle	25.2± 2.5	3.4 ± 2.7	1.35 ± 0.83	122.4 ± 29.7
OVX	B : Ca 2.0%, P 1.0%	vehicle	27.7± 3.4	3.5 ± 2.7	0.07 ± 1.39	115.6 ± 11.6
OVX	C : Ca 4.0%, P 1.0%	vehicle	27.8± 4.4	3.8 ± 2.9	0.31 ± 1.53	79.7 ± 16.1
OVX	D : Ca 6.0%, P 1.0%	vehicle	27.9± 6.6	3.8 ± 3.9	0.57 ± 2.76	141.4 ± 41.3
OVX	E : Ca 2.0%, P 1.8%	vehicle	22.3± 1.9	3.2 ± 9.3	2.18 ± 0.95	119.5 ± 30.0
OVX	F : Ca 4.0%, P 3.5%	vehicle	23.2± 3.2	3.2 ± 2.8	1.80 ± 1.36	128.9 ± 35.2
OVX	G : Ca 6.0%, P 5.2%	vehicle	20.0± 3.3**	2.9 ± 0.3**	2.79 ± 0.97*	132.3 ± 24.6*
OVX	A : Ca 1.2%, P 1.0%	ALF 0.025μg/kg	26.3± 3.9	3.6 ± 0.3	0.94 ± 1.27	70.3 ± 8.2
OVX	A : Ca 1.2%, P 1.0%	ALF 0.05μg/kg	28.8± 5.0	3.8 ± 0.4	-0.40 ± 1.53	55.0 ± 17.7
OVX	A : Ca 1.2%, P 1.0%	ALF 0.1μg/kg	34.5± 3.4**	4.3 ± 0.3***	-2.15 ± 1.37**	33.2 ± 5.6

BV/TV: bone volume, Tb.N: trabecular number, TBPf: trabecular bone pattern factor,
SMI: structure model index
Mean±SD (n=6-7) *p<0.05, **p<0.01, ***p<0.001 vs. 1.2%Ca OVX-control group (Dunnett's t test)

Fig. 6

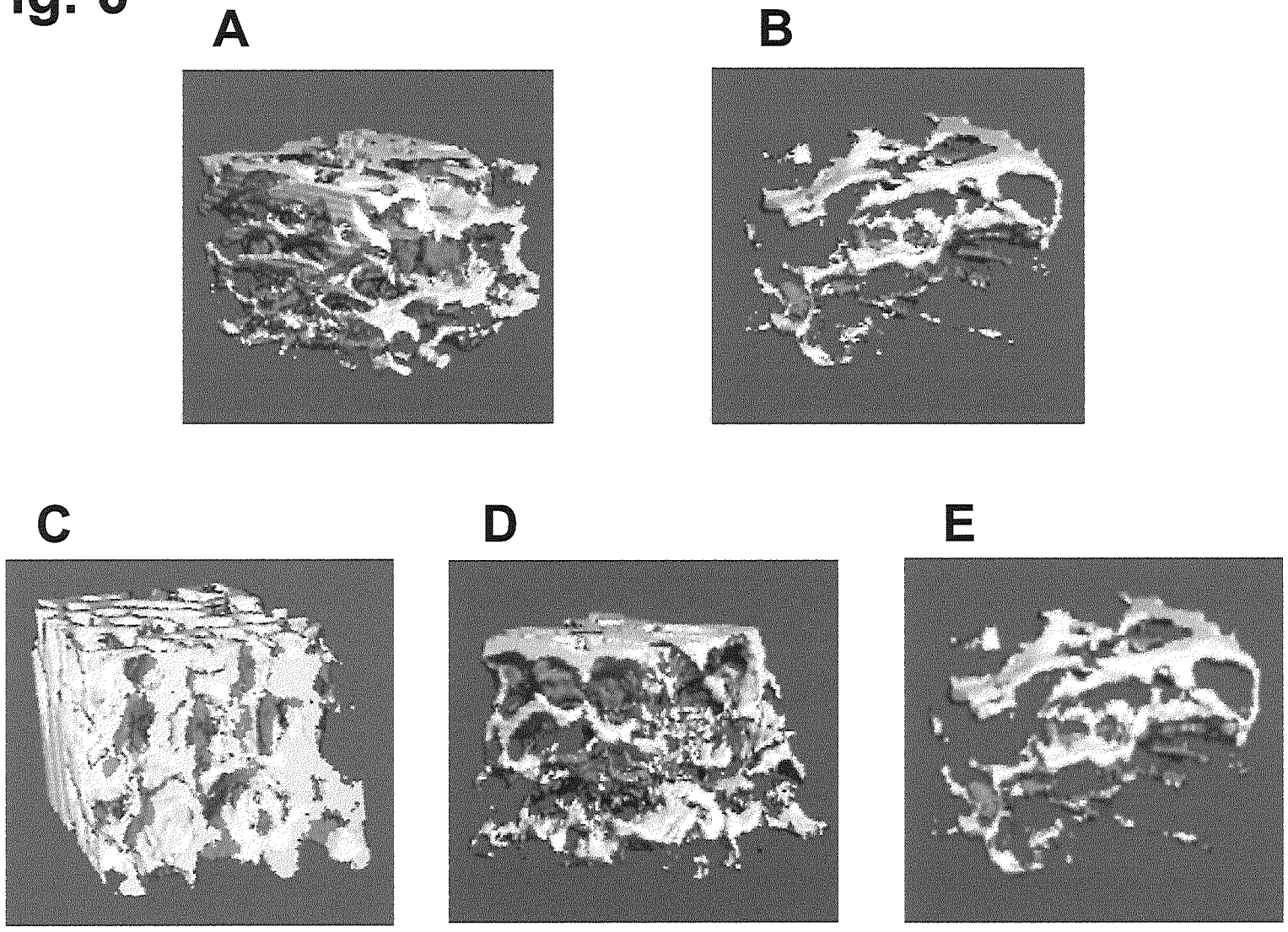

J Bone Miner Metab (2005) 23[Suppl]:115–121

INVITED PAPER

Masako Ito

Assessment of bone quality using micro-computed tomography (micro-CT) and synchrotron micro-CT

Abstract The latest micro-computed tomography (micro-CT) can provide ultrahigh-resolution images with resolution of less than 10 μm. Geometric three-dimensional (3-D) parameters, including the orientation, shape, and connectivity of trabeculae, are particularly helpful in understanding complex 3-D structure. Micro-CT is helpful for studying bone changes in various pathophysiological states and assessing changes in microarchitecture after treatment with antiosteoporotic agents. Trabecular microarchitecture is strongly related to bone strength, and 3-D micro-CT data can be used to assess bone biomechanical properties with the help of finite-element analysis. High photon flux from synchrotron X-ray sources reveals precise bone surface structure, and the monochromaticity of the beam is suitable for performing accurate density measurements. The preliminary results of an in vivo study of microarchitecture are also shown. Human vertebral microstructure can be revealed using multidetector row CT at a resolution of 200 × 200 × 300 μm. Analysis using high-resolution CT microstructure was found to be more useful in identifying subjects at high risk of fracture than clinical bone density measurements using dual X-ray absorptiometry.

Key words Microarchitecture · Micro-computed tomography (micro-CT) · Synchrotron radiation CT (SR-CT) · Bone mineralization · Finite-element analysis (FEA)

Introduction

The latest micro-computed tomography (micro-CT) can provide ultrahigh-resolution images with resolution of less than 10 μm. Geometric three-dimensional (3-D) parameters including the orientation, shape, and connectivity of trabeculae are particularly helpful in understanding complicated 3-D structure (Fig. 1). Histomorphometric parameters including bone volume fraction (BV/TV), trabecular thickness (Tb.Th), trabecular separation (Tb.Sp), and trabecular number (Tb.N) can be calculated directly and three-dimensionally [1]. The shape and magnitude of the orientation of trabeculae can be quantified as the structure model index (SMI) [2] or the degree of anisotropy (DA). Connectivity density [3] is a topological parameter that is used to estimate the number of trabecular connections per cubic millimeter (Fig. 1). Synchrotron radiation CT is a promising method for revealing precise trabecular structure and grade of mineralization. This review summarizes what we have learned from various studies using small animals.

M. Ito (✉)
Department of Radiology, Nagasaki University School of Medicine, 1-7-1 Sakamoto, Nagasaki 852-8501, Japan
Tel. +81-95-849-7354; Fax +81-95-849-7357
e-mail: masako@net.nagasaki-u.ac.jp

Microstructural changes resulting from different mechanisms of bone loss

An experimental study using ovariectomized (OVX) rats showed estrogen deficiency-induced trabecular deterioration, manifested as decreases in BV/TV, Tb.N, and connectivity density and increases in Tb.Sp and SMI (increases in the ratio of platelike trabeculae) compared to the sham-operated group [4]. Tb.Th does not always significantly decrease, probably because changes in this parameter depend on the duration of estrogen deficiency or the age of the animals, and its detection depends on the spatial resolution of micro-CT. DA increased after OVX, indicating that trabecular resorption occurs heterogeneously with preservation of the longitudinal trabeculae and disappearance or thinning of the transverse trabeculae. This is attributed to the fact that longitudinal trabeculae are oriented to resist axial loading, whereas transverse trabeculae are not.

In contrast, sciatic neurectomized (NX) rats showed marked trabecular deterioration. However, in this case the DA decreases, in contrast to OVX rats, because immobilization induces a decrease in the trabeculae without the effect of loading. The study suggests that the increase in DA associated with decreased bone mass results from adapta-

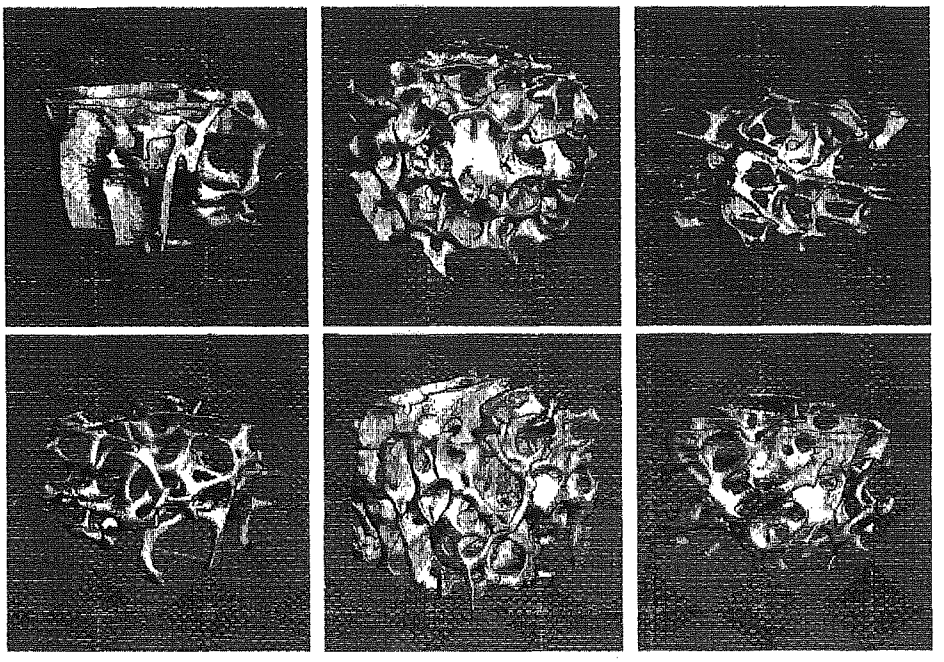

Fig. 1. Nonmetric parameters: structure model index (SMI) shape of trabecula (*left*), degree of anisotropy (DA) orientation of trabecula (center), and connectivity density (*right*)

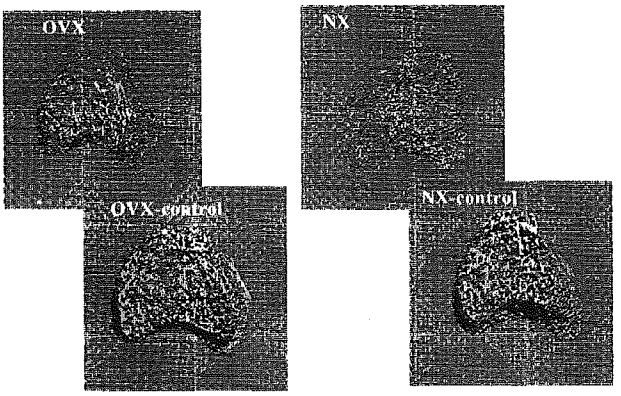

Fig. 2. Three-dimensional tibial trabecular micro-computed tomography (micro-CT) images from ovariectomized (OVX) and neurectomized (NX) rats: 3-D trabecular microstructure of OVX (*upper, left*), and NX (*upper, right*) rats and their respective control (*lower images*)

tion to loading, which maintains mechanical strength even with a small amount of bone mass. The decrease in cortical area is more prominent in the NX than in the OVX rats [5]. 3-D images in the NX rats showed flakelike trabeculae whereas those in the OVX rats demonstrated decreased trabeculae, predominantly in the central part of the tibia, but with preservation of trabecular shape (Fig. 2) [5].

Relationship between microstructure and biomechanical strength

Three-dimensional trabecular structure is strongly correlated to the biomechanical strength of bone (Fig. 3).

Effects of antiosteoporotic agents on trabecular microstructure

The efficacy of some antiosteoporotic agents was assessed using μ-CT20 (Scanco Medical, Bassendorf, Switzerland) [6]. It is difficult to compare changes in microstructure between pre- and posttreatment animal studies because these experiments had different individual protocols, using rats of different strains and different ages. To compare the efficacy of antiosteoporotic agents including human parathyroid hormone (hPTH) [7], menatetrenone [4], alfacalcidol [4], and three bisphosphinates (etidronate, alendronate, and incadronate), polar diagrams were prepared to demonstrate changes in several microstructural parameters, using sham-control as 200% and OVX-control as 100% (Fig. 4).

These polar diagrams indicate the differing effects of antiresorptive and bone-forming agents on microstructure. The bone-forming agents seem to have a stronger effect on thickening the trabeculae compared to the antiresorptive agents (bisphosphonates), while antiresorptive agents seem to maintain existing structure in a balanced manner.

Micro-finite-element analysis (micro-FEA)

Finite-element analysis (FEA) is a promising method for revealing the stress distribution of loaded bone, and this method can provide beneficial information about the mechanism of bone fracture. We developed an FEA system to evaluate the relationship between microstructure and mechanical properties. Using this system, we performed the following studies. Evaluation of the mechanical contri-

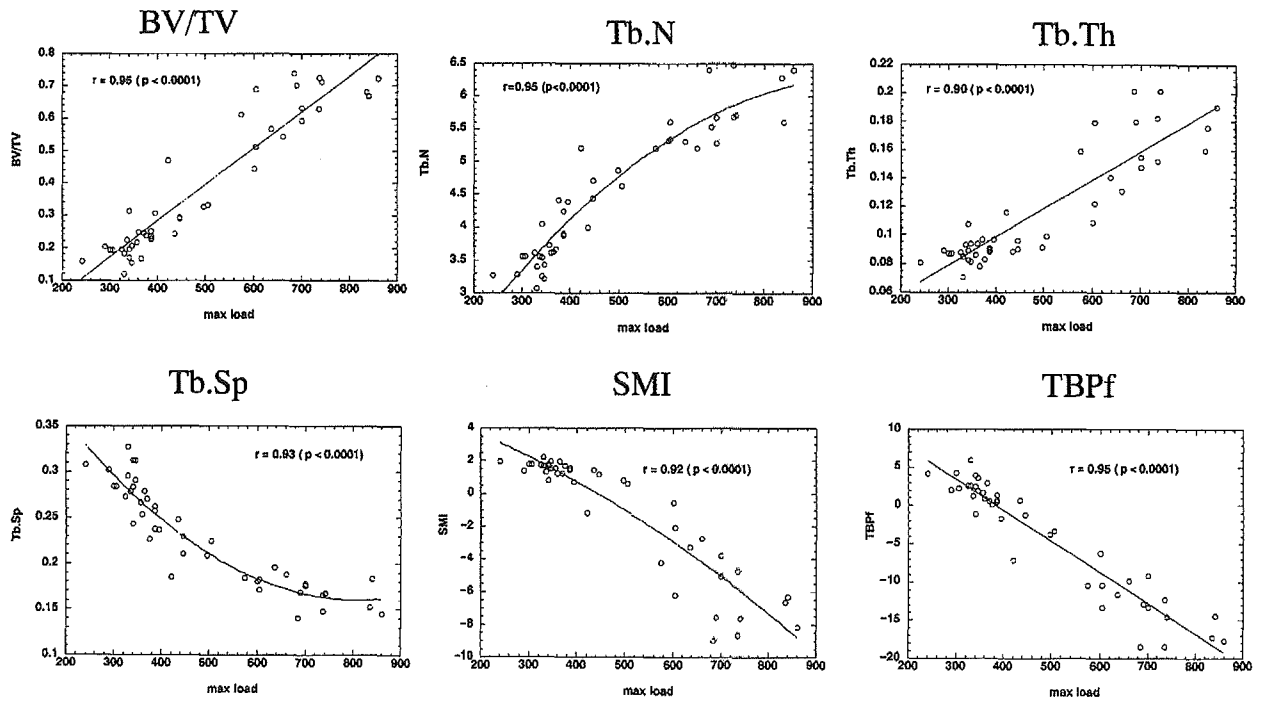

Fig. 3. Relationships between microstructural parameters and ultimate load. Microstructural parameters are *BV/TV*, bone volume fraction; *Tb.N*, trabecular number; *Tb.Th*, trabecular thickness; *Tb.Sp*, trabecular separation; *SMI*, structure model index; and *TBPf*, trabecular bone pattern factor

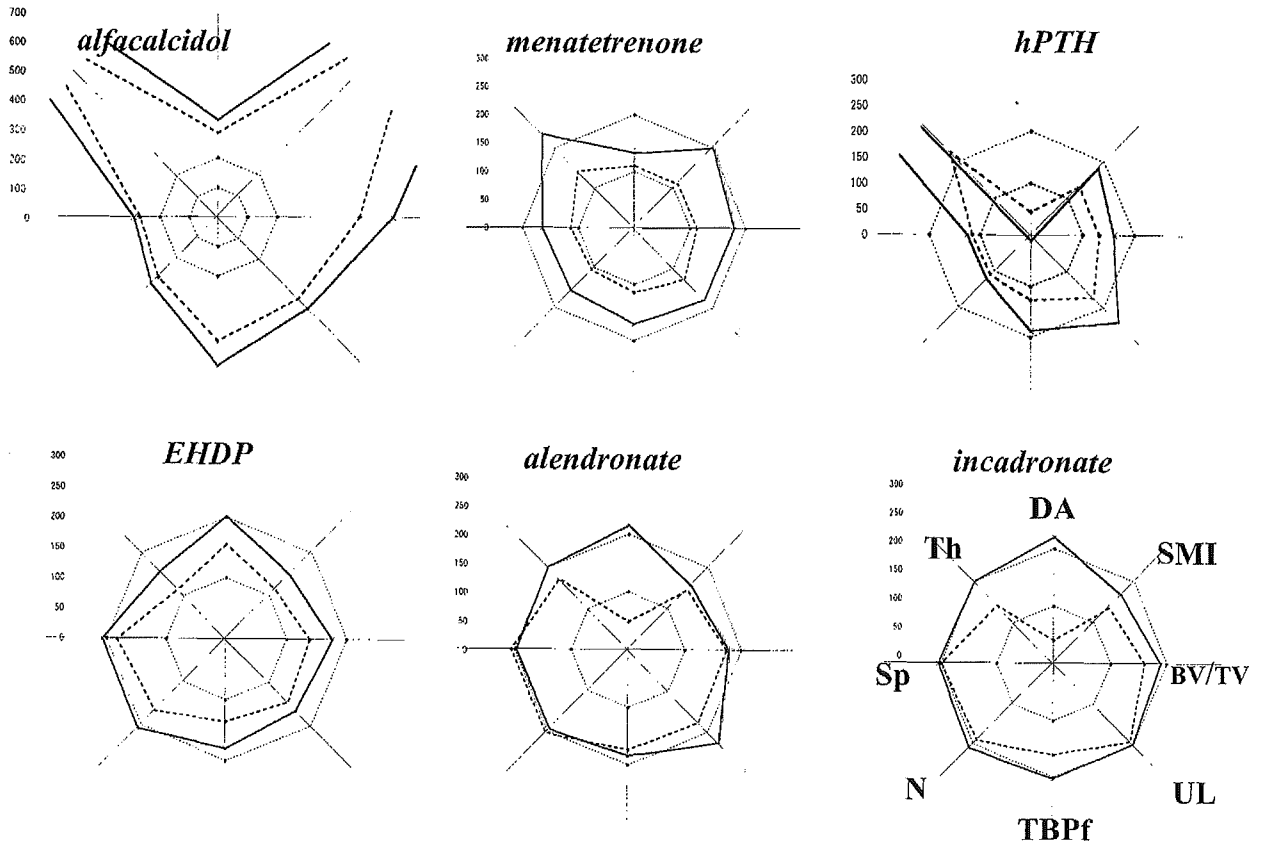

Fig. 4. Polar diagrams representing changes in the structural parameters of rat vertebrae with administration of the following antiosteoporotic agents; alfacalcidol (0.05, 0.1 μg/kg × 6 months), menatetrenone (3, 30 μg/kg × 6 months), human parathyroid hormone (hPTH) (90 mg/kg ↘ 3 months + vehicle ↗ 3 months, 90 mg/kg × 6 months), and three bisphosphonates: etidronate [2, 8 mg/kg (× 2 weeks + no treatment × 10 weeks) ×2], alendronate (20, 80 μg/kg × 3 months), and incadronate (20, 80 μg/kg × 3 months). *EHDP*, etidronate; *BV/TV*, bone volume fraction; *SMI*, structure model index; *DA*, degree of anisotropy; *Tb.Th*, trabecular thickness; *Tb.Sp*, trabecular separation; *Tb.N*, trabecular number; *TBPf*, trabecular bone pattern factor

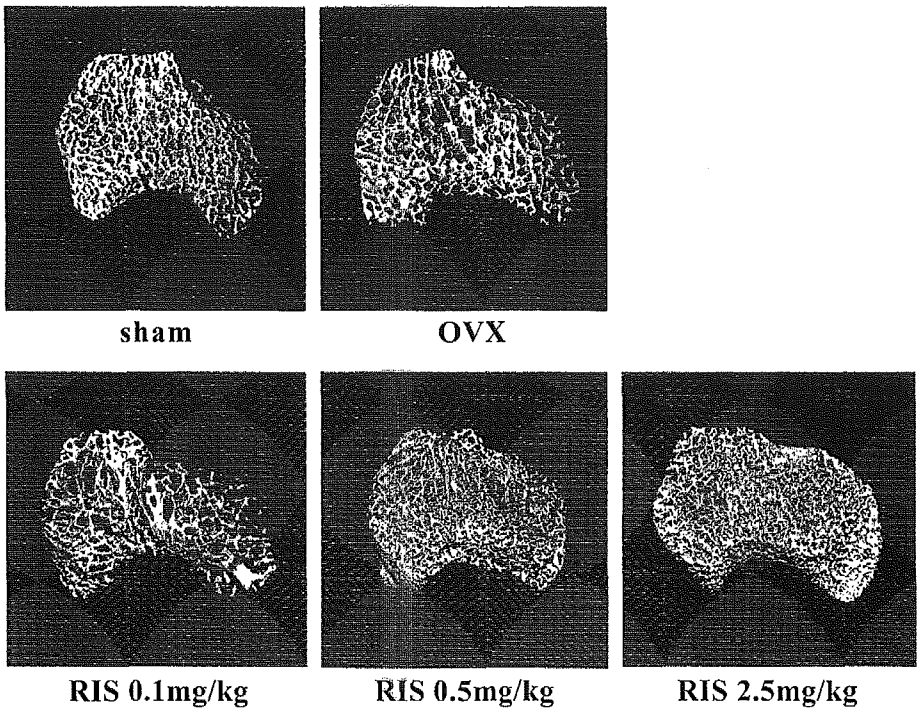

Fig. 5. Three-dimensional trabecular micro-CT of tibia show representative images of sham, OVX vehicle, and OVX rats treated with risedronate (0.1, 0.5, 2.5 mg/kg)

bution of the spongiosa and cortex to the whole rat vertebra showed that the trabecular microstructure has a significant relationship to bone strength; however, in bone with deteriorated trabecular microstructure, strength depends mainly on the cortical component [8]. The effect of risedronate on the trabecular microstructure of ovariectomized rat tibiae was evaluated using micro-CT, and effect on its biomechanical properties was assessed by FEA. Fifty 18-week-old rats underwent sham operation (n = 10) or ovariectomy (OVX) (n = 40). The OVX rats were further divided into four groups (n = 10 for each group) treated with risedronate at doses of 0, 0.1, 0.5 or 2.5 mg/kg for 9 months.

OVX caused deterioration of the three-dimensional trabecular microstructure, whereas treatment of OVX rats with risedronate at 0.5 and 2.5 mg/kg prevented these deleterious microstructural changes (Fig. 5). To assess biomechanical properties, the prepared cubic bone volume was directly incorporated into an FE model to determine the elastic properties of the trabecular network using a voxel-based FEA program. The 3-D binary image was used to generate an FE model by converting the pixels of the solid phase to correspondingly shaped 8-node brick elements [9]. Using a specially designed FE-solver (Scanco Medical FE-software, version 1.1), compression and shear tests were simulated in the three orthogonal directions. For these simulations, the tissue elastic properties were set as linear elastic and isotropic with a Young's modulus of 10 GPa and a Poisson's ratio of 0.3 [10]. The stiffness matrix was calculated using the results of these six simulations [11]. An optimization procedure was then used to find a new coordinate system aligned with the best orthogonal symmetry directions. The stiffness matrix was rotated to this new orthogonal coordinate system, and the Young's moduli as well as shear moduli were calculated in these principal directions. Figure 6 shows the 3-D image of the original microstructure (B) and the corresponding 3-D image of von Mises stress distribution (C).

Table 1 shows Young's and shear moduli as well as Poisson's ratio in the primary directions in OVX rats and risedronate-treated OVX rats. OVX caused a significant decrease in Young's modulus, and tended to decrease shear modulus and to increase Poisson's ratio, compared with the sham group. Treatment with risedronate at the dose of 2.5 mg/kg significantly increased Young's and shear moduli even above the values of the sham group, and decreased Poisson's ratio below the value of the sham group. These studies show that FEA is useful for assessing the biomechanical properties of bone without bone destruction, especially on extracted trabecular bone [12].

Synchrotron radiation CT (SR-CT)

Micro-CT has a limited ability to delineate the detail of a trabecular surface (resorption cavity) or mineralized tissue because of beam-hardening artifacts in the reconstructed images due to the stronger attenuation of soft X-rays in the sample. Synchrotron radiation (SR) provides an intense, laser-like collimated light in the range from infrared to hard X-rays. The high photon flux from synchrotron X-ray

Table 1. Biomechanical parameters in the sham and OVX rats treated with risedronate

Group	Young's modulus	*P*		Shear modulus	*P*	
Sham	1074 ± 454			208 ± 154		
OVX vehicle	361 ± 300		††	82 ± 105		ns
OVX risedronate 0.1 mg/kg/day	527 ± 257	ns	††	72 ± 67	ns	†
OVX risedronate 0.5 mg/kg/day	638 ± 161	ns	†	93 ± 125	ns	ns
OVX risedronate 2.5 mg/kg/day	3691 ± 1555	***	†††	1163 ± 682	***	†††

OVX, ovariectomy
* $P < 0.05$, ** $P < 0.01$, *** $P < 0.001$, significantly different from OVX vehicle group; † $P < 0.05$, †† $P < 0.01$, ††† $P < 0.001$, significantly different from sham group

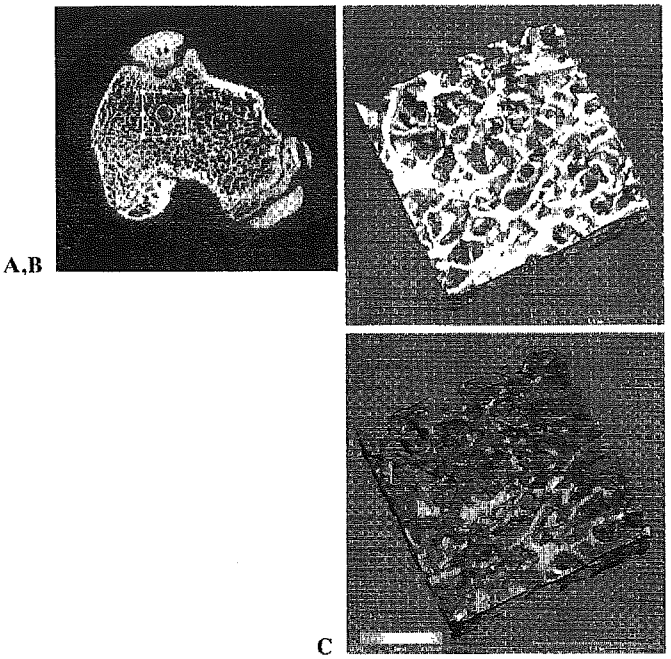

Fig. 6. Compression and shear simulation of the three orthogonal directions. **A** Region of proximal tibia that was extracted for finite-element analysis. The *circle* in the center of the cubic region indicates the region used for calculating the degree of anisotropy (DA). **B** Original 3-D micro-CT image (upper half of the total region). **C** 3-D distribution image of von Mises stress (upper half of the total region)

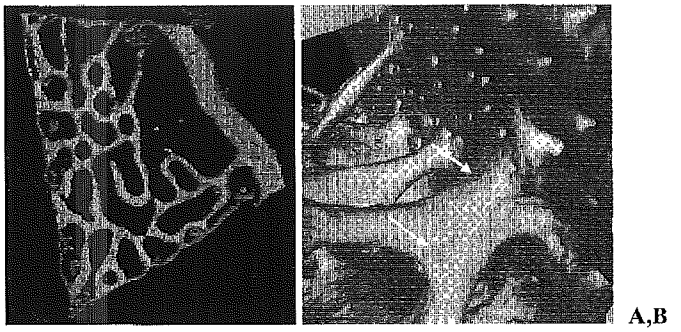

Fig. 7. 2-D and 3-D trabecular microstructure synchrotron radiation CT (SR-CT) images of rat vertebra. **A** 2-D image shows the sharp border of the trabeculae without visible partial volume effect. **B** 3-D image shows shallow concavities in the trabecular surfaces (*arrows*)

sources and the small angular source size with negligible geometric blur make it possible to obtain images with high spatial resolution and a high signal-to-noise ratio (Fig. 7). The monochromaticity of the beam is suitable for performing accurate density measurements. White-beam SR can reveal different densities according to different grades of mineralization and can precisely reveal bone surface structure. The comparison of SR-CT images with contact microradiography (CMR) (Fig. 8) or scanning electron microscopy (SEM) images confirms its ability to visualize details such as resorption cavities and mineralization in bone [13].

In addition, SR-CT can provide elemental (calcium) mapping. We have developed a method to visualize calcium (Ca) density in bone using SR-CT to observe differences in 3-D Ca density distribution. Because mass attenuation coefficients change according to X-ray energy, the coefficients of Ca and carbon (C) can be obtained using energy values of 10, 15, 17, 25, and 40 KeV. Ca and C density are then calculated using the following formulae; $\mu = (\mu_{Ca}/\rho_0)\rho_{Ca} + (\mu_C/\rho_0)\rho_C$, where μ is the CT value, μ_{Ca}/ρ_0 and μ_C/ρ_0 are the mass attenuation coefficients of calcium and carbon, and ρ_{Ca} and ρ_C are the densities of calcium and carbon, respectively.

Visualization and analysis of trabecular microstructure in vivo using multidetector row CT

Using multidetector row CT (MDCT), vertebral trabecular microstructure can be visualized in vivo. The spatial resolution of the image is 200 × 200 × 300 μm. In our preliminary study, the subjects were 23 women with fresh vertebral fractures and 27 women without fractures (there were no significant differences between the groups with respect to age or age at menopause). Logistic regression analysis showed that microstructural parameters measured by MDCT such as BV/TV, Euler's number, and trabecular bone pattern factor (TBPf) had higher odds ratios than spinal bone mineral density (BMD) measured by dual-energy X-ray aborptiometry (DXA). This finding indicates that analysis of human vertebral microstructure by MDCT is a more sensitive way to predict the risk of fracture than BMD measured by DXA. The 3-D images of the whole bone are shown in Fig. 9.

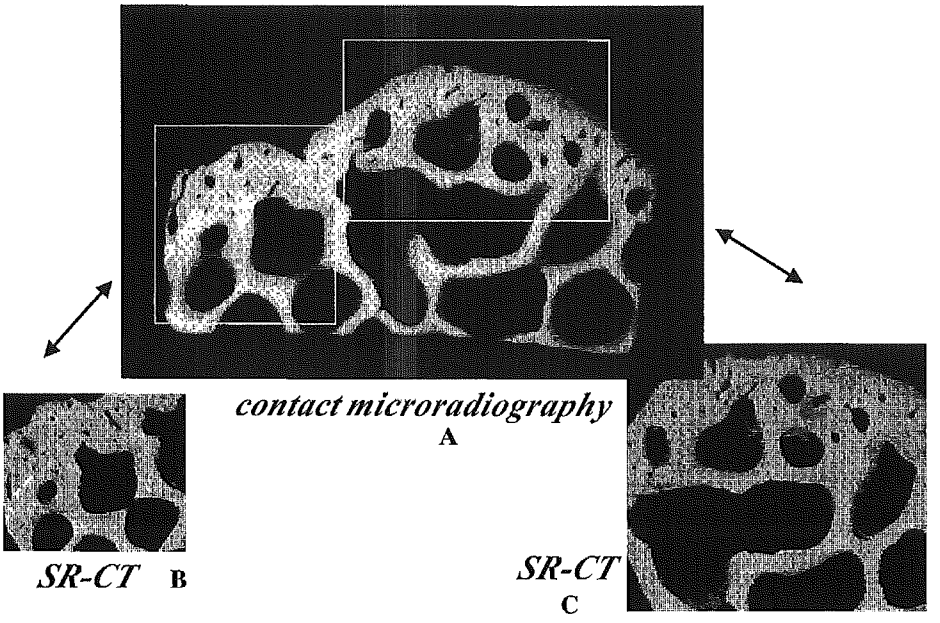

Fig. 8. 2-D SR-CT and contact microradiography (CMR) images of vertebral bone in the minipig. Different densities can be detected in the surface of the trabeculae by SR-CT (**B, C**) as well as by CMR (**A**)

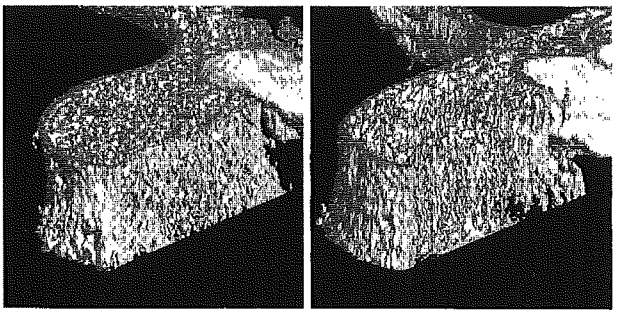

Fig. 9. 3-D images of the third lumbar spine. The CT image on the *left* is from a 62-year-old woman without fracture; the CT image on the *right* is from a 62-year-old women with a fresh vertebral fracture (T12)

Summary

1. Micro-CT provides a method of visualizing 3-D structure for the assessment of the effects of antiosteoporotic agents in relation to bone strength.
2. SR-CT is a potential method for assessing the quality of bone.
3. Micro-FEA is useful for investigating biomechanical competence without bone destruction.
4. We developed a microstructure analysis system using MDCT to evaluate bone strength in vivo.

Acknowledgments I am grateful to Dr. Kyoji Ikeda (Department of Bone and Joint Disease, The Research Institute, National Center for Geriatrics and Gerontology), Dr. Toshitaka Nakamura (Department of Orthopaedic Surgery, School of Medicine, University of Occupational and Environmental Health), Ms. Ayako Shiraishi and Ms. Sayumi Higashi in Chugai Pharmaceutical Co., Ltd., and Mr. Tomoyuki Tanaka and Ms. Takashi Katsumata in Sumitomo Pharmaceutical Co., Ltd. for their collaboration. I thank Mr. Jun Kono (Department of Radiology, Nagasaki Saiseikai Hospital) for his assistance. This study was supported in part by the Program for Promotion of Fundamental Studies in Health Science of the Organization for Pharmaceutical Safety and Research of Japan (Masako Ito [No. MF-14]).

References

1. Hildebrand T, Rüegsegger P (1997) A new method for the model-independent assessment of thickness in three-dimensional images. J Microsc 185:67–75
2. Hildebrand T, Rüegsegger P (1997) Quantification of bone microarchitecture with the structure model index. Comput Methods Biomech Biomed Eng 1:15–23
3. Odgaard A, Gundersen HJ (1993) Quantification of connectivity in cancellous bone, with special emphasis on 3-D reconstructions. Bone 14:173–182
4. Shiraishi A, Higashi S, Masaki T, Saito M, Ito M, Ikeda S, Nakamura T (2002) A Comparison of alfacalcidol and menatetrenone for the treatment of bone loss in an ovariectomized rat model of osteoporosis. Calcif Tissue Int 71:69–71
5. Ito M, Nishida A, Nakamura T, Uetani M, Hayashi K (2002) Differences of three-dimensional trabecular microstructure in osteopenic rat models caused by ovariectomy and neurectomy. Bone 30:594–598
6. Ruegsegger P, Koller B, Müller R (1996) A microtomographic system for the non-destructive evaluation of bone architecture. Calcif Tissue Int 58:24–29
7. Okimoto N, Tsurukami H, Okazaki Y, Nishida S, Sakai A, Ohnishi H, Hori M, Yasukawa K, Nakamura T (1998) Effects of a weekly injection of human parathyroid hormone (1-34) and withdrawal on bone mass, strength, and turnover in mature ovariectomized rats. Bone 22:523–531
8. Ito M, Nishida A, Koga A, Ikeda S, Shiraishi A, Uetani M, Hayashi K, Nakamura T (2002) Contribution of trabecular and cortical components to the mechanical properties of bone and their regulating parameters. Bone 31:351–358
9. van Rietbergen B, Weinans H, Huiskes R, Odgaard A (1995) A new method to determine trabecular bone elastic properties and

loading using micromechanical finite-element models. J Biomech 28:69–81
10. van Rietbergen B, Huiskes R, Weinans H, Odgaard A, Kabel J (1995) The role of trabecular architecture in the anisotropic mechanical properties of bone. In: Odgaard A, Weinans H (eds) Bone Structure and Remodeling. World Scientific, Singapore, pp 137–145
11. van Rietbergen B, Odgaard A, Kabel J, Huiskes R (1996) Direct mechanics assessment of elastic symmetries and properties of trabecular bone architecture. J Biomech 29:1653–1657
12. Ito M, Nishida A, Aoyagi K, Uetani M, Hayashi K, Kawase M (2005) Effects of risedronate on trabecular microstructure and biomechanical properties in ovariectomized rat tibia. Osteoporosis Int. DOI. 10.1007/s00198-004-1802-3
13. Ito M, Ejiri S, Jinnai H, Kono J, Ikeda S, Nishida A, Uesugi K, Yagi N, Tanaka M, Hayashi K (2003) Bone structure and mineralization demonstrated using synchrotron radiation computed tomography (SR-CT) in animal models: preliminary findings. J Bone Miner Metab 21:287–293

JOURNAL OF BONE AND MINERAL RESEARCH
Volume 20, Number 10, 2005
Published online on June 20, 2005; doi: 10.1359/JBMR.050610

Multi-Detector Row CT Imaging of Vertebral Microstructure for Evaluation of Fracture Risk

Masako Ito,[1] Kyoji Ikeda,[2] Masahiko Nishiguchi,[3] Hiroyuki Shindo,[4] Masataka Uetani,[1] Takayuki Hosoi,[5] and Hajime Orimo[6]

ABSTRACT: We applied MDCT for in vivo evaluation of the microarchitecture of human vertebrae. Microstructure parameters, such as structure model index, Euler's number, and bone volume fraction, revealed higher relative risk for prevalent vertebral fracture than did BMD obtained by DXA. Thus, microstructure analysis by MDCT, together with simultaneously obtained volumetric BMD values, is useful for clinical assessment of fracture risk.

Introduction: BMD measurement by DXA alone has limitations in predicting fracture, and methods for clinical assessment of bone quality, such as microstructure, are awaited. This study was undertaken to examine the applicability of multidetector row CT (MDCT) for in vivo evaluation of trabecular microstructure.
Materials and Methods: Optimal conditions for MDCT scanning were determined at a spatial resolution of 250 × 250 × 500 μm, using μCT data of excised human vertebra specimens as a reference. We analyzed the trabecular microstructure of the vertebrae of 82 postmenopausal women (55–76 years old), including 39 women with and 43 without a recent vertebral fracture.
Results: Microstructure indices obtained by MDCT scanning revealed higher relative risk for prevalent vertebral fracture (OR: 16.0 for structure model index, 13.6 for bone volume fraction, and 13.1 for Euler's number) than did spinal BMD obtained by DXA (OR: 4.8). MDCT could also provide volumetric BMD data, which had higher diagnostic value (OR: 12.7) than did DXA.
Conclusion: Vertebral microarchitecture can be visualized by MDCT, and microstructure parameters obtained by MDCT, together with volumetric BMD, provided better diagnostic performance for assessing fracture risk than DXA measurement.
J Bone Miner Res 2005;20:1828–1836. Published online on June 20, 2005; doi: 10.1359/JBMR.050610

Key words: osteoporosis, fracture, CT, microstructure

INTRODUCTION

BMD MEASUREMENTS ARE widely used for the diagnosis of osteoporosis and for the evaluation of the efficacy of treatment for this disease. However, BMD measurements alone have limitations in predicting fracture. In fact, a recent study indicates that 82% of postmenopausal women with fracture had BMD measurements in the osteopenic, not osteoporotic, range.[1] In addition, there is accumulating evidence that only a small fraction of the reduction in fracture with therapy can be accounted for by the increase in BMD.[2] These results suggest that factors other than BMD, such as bone structure and turnover rate of bone remodeling, contribute to bone fragility.[3]

μCT enables us to evaluate, at an ultra-high resolution, the microstructure of bone samples without destroying them, but it cannot be used in vivo. Studies by high-resolution CT, using different texture analysis methods as well as thresholding techniques, have reported results on its use.[4–6] However, the in-plane spatial resolution of conventional high-resolution CT is only 400 × 400 μm, and this conventional CT only gives information on the characteristic texture of a structure, such as rough versus smooth, homogeneous versus heterogeneous, or high versus low orientation of trabecular distribution. The reason for this is that the trabecular structure is subjected to partial-volume effects. Spiral CT has a higher resolution than conventional CT; however, it is subjected to scan-axis partial volume effects. Multidetector row CT (MDCT) is a new technique that has a substantially higher spatial resolution than standard spiral CT (i.e., it provides an in-plane spatial resolution of 250 μm and a minimum slice thickness of 500 μm) and thus promises to improve the assessment of trabecular bone structure.

The authors have no conflict of interest.

[1]Department of Radiology, Nagasaki University School of Medicine, Nagasaki, Japan; [2]Department of Bone and Joint Disease, The Research Institute, National Center for Geriatrics and Gerontology, Obu, Aichi, Japan; [3]Department of Orthopedic Surgery, Japan Ekisai-kai Nagasaki Hospital, Nagasaki, Japan; [4]Department of Orthopedic Surgery, Nagasaki University School of Medicine, Nagasaki, Japan; [5]Department of Internal Medicine, Tokyo Metropolitan Institute of Gerontology and Geriatric Hospital, Tokyo, Japan; [6]Health Science University, Tokyo, Japan.

This study was undertaken to apply MDCT for 3D imaging of the trabecular microarchitecture of human vertebrae and to evaluate the use of the microstructure parameters obtained by MDCT for the assessment of fracture risk in postmenopausal women.

MATERIALS AND METHODS

Specimen study

Specimens: Five formalin-fixed specimens of vertebrae of female cadavers (62–83 years of age at the time of death) were obtained from Tokyo Metropolitan Institute of Gerontology and Geriatrics Hospital. These vertebrae were used to define the appropriate scanning milli-ampere second value within clinically available values that revealed trabecular microstructure with a low signal-to-noise ratio. To compare the MDCT images with those obtained by μCT, we mounted the excised vertebral specimens on a sample holder of 40 mm diameter filled with an 8% gelatinous solution containing 88% protein, 1% mineral, and 11% water to keep the specimens steady. Specimens that contained air on CT images were excluded. The study protocol was approved by the ethical committee of Tokyo Metropolitan Institute of Gerontology and Geriatrics.

Imaging by μCT: μCT scanning was performed ex vivo on excised human vertebrae to validate MDCT images and data. A μCT apparatus (μCT40) and its analysis software were purchased from SCANCO Medical (Basserdorf, Switzerland).[7] Details of an earlier model (μCT20) were described previously.[8] The process was piloted by an Alpha DS10 workstation (Compaq Computer Corp.), and an open VMS system in a cluster configuration was used to perform 3D analysis. Each specimen was positioned as so to permit scanning of 600 slices with 40-μm increments with a spatial resolution of ~40 μm.

Imaging by MDCT: After μCT scanning, bone specimens in the holder were placed in a 20-cm thickness water-equivalent solid phantom (Standard Grade Solid Water Gammex 457; GAMMEX RMI) and scanned by MDCT. Axial CT images with a collimation of 0.5 mm, a table feed of 2 mm, and a reconstruction index of 0.3 mm were obtained with a MDCT system having four detectors (SOMATOM plus 4 Volume Zoom; Siemens, Erlangen, Germany). An ultra-high spatial resolution kernel was applied (head, filter H 70 very sharp). CT scanning of excised vertebra was performed with the following scanning conditions: field of view (FOV) of 100 mm and pixel matrix of 512 × 512, leading to a maximal spatial resolution of ~250 × 250 × 500 μm^3.

We first determined optimal conditions for MDCT scanning by using excised human vertebrae and compared the MDCT data with those obtained by μCT as a reference. Figure 1 shows images of an excised human vertebra obtained by μCT (Fig. 1A, with the volume of interest shown by a square), high-resolution CT images obtained by MDCT at 200, 250, and 300 mAs (Fig. 1B), their binarized images (Fig. 1C), and reconstructed 3D images (Fig. 1D). Scanning at 350 mAs was not performed because of overload of X-ray tube use for clinical cases. Measurements were repeated at the same position five times, and precision of repeated measurements was 2.35 ± 0.56% for bone volume/total volume (BV/TV), 2.21 ± 2.91% for trabecular number (Tb.N), 3,17 ± 3.28% for trabecular thickness (Tb.Th), 3.62 ± 1.29% for trabecular separation (Tb.Sp), 7.45 ± 1.26% for Euler's number, 4,08 ± 1.48% for structural model index (SMI), and 4.21 ± 1.42% for fractal dimension (n = 3 each).

Structure analysis: Both MDCT image data and μCT data were transferred to a workstation (Precision 360; Dell), and structural indices were calculated using a 3D image analysis system (TRI/3D-BON; RATOC System Engineering Co., Tokyo, Japan). To compare the parameters between μCT images and MDCT images, we defined the volume of interest (VOI) in μCT images first, and then adjusted it for MDCT images with reference to the VOI in μCT images. Grayscale images were segmented by using a median filter to remove noise with a fixed threshold to extract mineralized bone components. We used a standardized method of image thresholding based on the density histogram of a selected region of interest (ROI) to ensure consistency in the image thresholding across all subjects studied. Isolated small particles in the marrow space and isolated small holes in bone were removed by using a cluster-labeling algorithm.

Trabecular microstructure parameters were calculated in 3D as follows: bone volume (BV) was calculated using tetrahedrons corresponding to the enclosed volume of the triangulated surface. Total tissue volume (TV) was the entire volume of analysis, and apparent trabecular bone volume fraction (app BV/TV) was calculated from these values. Apparent trabecular thickness (app Tb.Th) was determined according to the method described by Hildebrand and Ruggsegger.[9] Apparent trabecular number (app Tb.N) and apparent trabecular separation (app Tb.Sp) were estimated based on the plate model.[10]

In addition to the computation of metric parameters, nonmetric parameters were calculated to obtain the 3D nature of the trabecular bone samples. Fractal dimensions of trabecular bone were measured as a representative of complexity using the box-counting method[11] that was developed in 3D. Connectivity was calculated by using the Euler method of Odgaard and Gundersen (Euler's number).[12] Degree of anisotropy (DA) was determined from the ratio between the maximal and minimal radii of the mean intercept length (MIL) ellipsoid.[13]

The interactive analysis time, including data examination, ROI definition, and image segmentation, was ~10 minutes for each type of data.

Biomechanical study

Specimens and microstructure analysis: Four femoral head specimens were obtained during surgery for femoral neck fracture at Nagasaki Rosai Hospital (2 men, 70 and 78 years of age; 2 women, 83 and 85 years of age). Surrounding soft tissues were removed, and 10-mm^3 specimens were prepared and stored at –20°C before use. The study protocol was approved by the ethical committee of Nagasaki Rosai Hospital.

These specimens were placed in an acrylic tank containing physiological saline solution and scanned by MDCT. Scanning direction was adjusted to the direction of loading

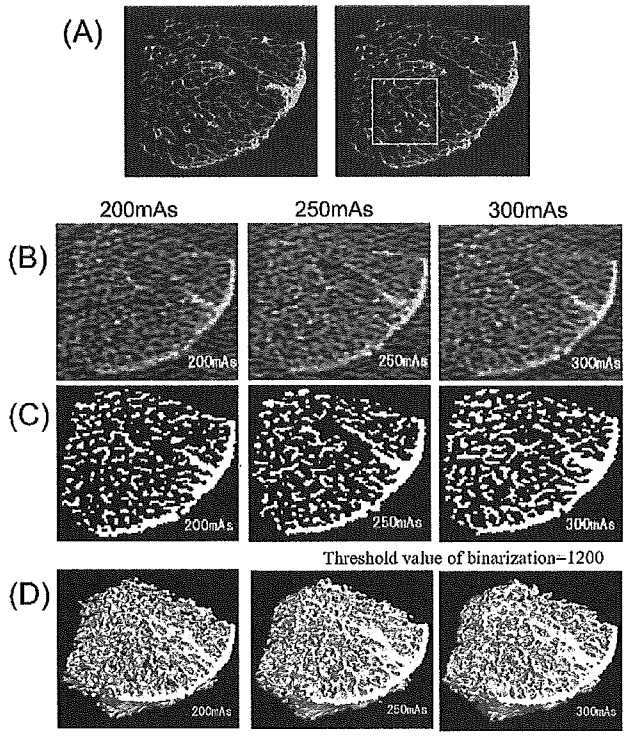

Threshold value	mAs	r	p
1120	200	0.656	ns
	250	0.487	ns
	300	0.959	< 0.01
1200	200	0.665	ns
	250	0.899	< 0.05
	300	0.979	< 0.005
1280	200	0.629	ns
	250	0.886	< 0.05
	300	0.959	< 0.05

FIG. 1. Visualization of spinal microstructure by MDCT scanning. Representative images of excised human vertebrae by (A) μCT image (volume of interest delimited by the square) and (B–D) MDCT images are shown. MDCT images were obtained under different conditions at 200, 250, and 300 mA; each CT image was analyzed at different threshold values (1120, 1200, and 1280). (B) Original 2D MDCT images at 200, 250, and 300 mA. (C) Binarized 2D CT images at 200, 250, and 300 mAs. (D) 3D CT images at 200, 250, and 300 mAs. The binarized and 3D images were prepared by using a threshold value of 1200. The linear correlations (r) and statistical significances (p) between apparent BV/TV measured by μCT and MDCT at 200, 250, and 300 mAs are also shown at the right.

in the biomechanical test. The scanning condition was the same as in the cadaver specimen study described above. Microstructure parameters were obtained for all of the specimens by the same procedure described above.

Determination of bone strength by compression test: Specimens were placed centrally on the compression testing fixture, which is able to hold the specimen stably in the cylinder and load only compressive direction without rotation or bending, and was attached to the materials-testing machine (Instron model 5582). A compression force was applied in a cranio-caudal direction using the fixture at a nominal deformation rate of 0.5 mm/minute and a sampling rate of 20 Hz. Crosshead displacement was recorded as specimen deformation. A load-deformation curve was displayed with a monitoring recorder linked to the tester in each specimen. The ultimate load (kgf) was obtained directly from the load-deformation curve.

Patient study

Patients: Spinal microarchitecture was examined in 82 postmenopausal women (55–76 years old, 65.3 ± 4.8 years) with MDCT scanning. Microstructure parameters were compared between 39 women who experienced their first spinal fracture during the previous 6 months (age: 66.2 ± 3.8 years old) and 43 women without fracture (age: 64.4 ± 5.5 years old) to assess the correlation between these parameters and fracture. Spinal fracture was defined according to the criteria proposed by Genant et al.[14] (i.e., vertebral deformity was considered as a fracture when at least a 20% reduction in anterior, middle, and/or posterior height and a 10% reduction in area were observed). Individuals who had had an osteoporotic fracture 6 months or more before the study were excluded, because bone structure would have been altered by the fracture. None of the postmenopausal women had received drugs affecting bone mass or bone metabolism within 6 months before the study. Nagasaki University ethics committee approved the protocol, and all subjects (i.e., fracture cases and controls) gave their informed consent.

BMD measurements: BMD of the lumbar spine (L_2–L_4) in antero-posterior (AP) projection was determined using DXA, and fractured vertebrae were excluded from the analysis. The obtained values were expressed as units of grams per centimeter squared for the projected area. Expert-EL (Lunar Corp., Madison, WI, USA) was used to measure the BMD of the lumbar spine. The CV (short-term precision) for L_2–L_4 was 1.1%.

To obtain volumetric BMD data by QCT, we scanned the patients simultaneously with MDCT using a bone mineral reference phantom (B-MAS2000; KYOTOKAGAKU Co.,

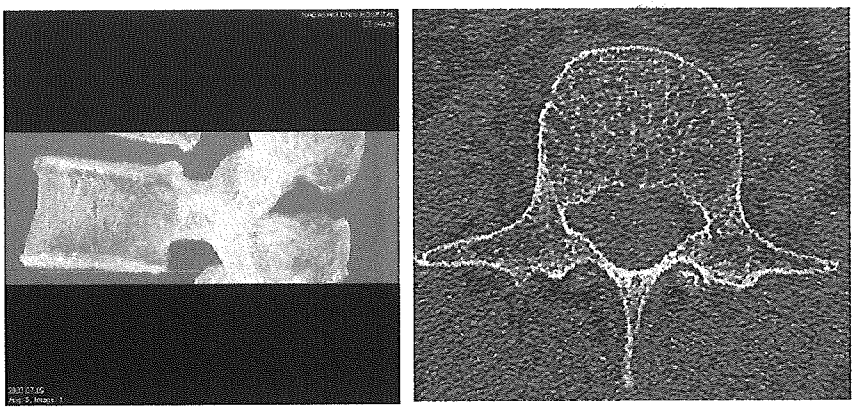

(A) (B)

FIG. 2. ROI for analysis of trabecular microstructure by MDCT. (A) The whole third lumbar spine including both endplates was scanned by MDCT. (B) The volume of interest (VOI) of 65 × 65 pixels in plane was defined in the anterior part of the spongiosa (delimited by the square) to avoid cortex and the basivertebral foramen.

Kyoto, Japan) containing calibration objects with equivalent densities of 0, 50, 100, 150, and 200 mg/cm^3 calcium hydroxyapatite. Reconstructed stacked 3D volume data of the vertebral body with reference phantom were used for the determination of volumetric BMD. VOI was defined in the same region for microstructure measurement of the reconstructed vertebral CT image.

Imaging by MDCT and structure analysis: The whole third lumbar spine including both endplates was scanned by MDCT, as shown in Fig. 2A. Patients were in the supine position for horizontal scanning of the vertebral body. The vertebral body was scanned under the appropriate X-ray condition, which was determined in the ex vivo cadaver study as described above. For the analysis of microstructure, the size of the VOI of 65 × 65 pixels in plane was defined (Fig. 2B); the total number of slices varied according to the size of the vertebral body. The VOI was defined manually within the internal part of the cancellous bone to avoid the cortex, the basivertebral foramen, and both endplates. The midline of the VOI in the x-axis in the axial image was in the center of the vertebral body, and the frontal edge on both sides of the VOI was just behind the cortex. The average number of slices was 43.8 ± 5.3 (range, 28–52 slices).

The procedure for structure analysis was the same as that for the cadaver specimen study described above. Samples from three patients were scanned five times on different days, using manually defined VOI; the precision was confirmed by the same operator. Precision of measurements of microstructure parameters was 0.67% for fractal dimension, 0.84% for Tb.Th, 1.13% for SMI, 2.04% for DA, 6.57% for Tb.N, 7.13% for BV/TV, 7.36% for Tb.Sp, and 12.30% for Euler's number.

Statistical analysis

Data analysis was performed with the software statistical package for Social Science, SPSS (SPSS, Chicago, IL, USA). Mean and SD of microstructure parameters and BMD were calculated for the postmenopausal women with or without fracture. The significance of differences between the two groups was calculated by ANOVA and posthoc test (Fisher's protected least significant difference [PLSD]), at the 95% significance level. Correlations of microstructure parameters or BMD with age or body weight of the subjects and correlations between microstructure parameters and BMD were assessed using linear regression analysis. Area under the curve (AUC) in receiver operator characteristic (ROC) analysis was generated to determine the diagnostic efficacy for detection of fracture cases. Additionally, the ORs per SD were calculated by logistic regression analysis to provide an estimate for the discriminatory capability of each variable for spinal fracture, as a single parameter or in combination with DXA or QCT value.

RESULTS

Specimen study

Optimal conditions for MDCT scanning: To determine the optimal conditions for MDCT scanning, we obtained vertebral specimens from cadavers and scanned them by both μCT (Fig. 1A) and MDCT (Figs. 1B–1D). Microstructure parameters were calculated at threshold values of 1120, 1200, and 1280 to binarize bone CT images. These values of threshold were numbers on a scale from 0 to 4290 according to linear attenuation, which has no units. As shown in Fig. 1 (right), at all three threshold levels, BV/TV obtained by μCT revealed the highest correlation with app BV/TV by MDCT at 300 mAs (r = 0.979, $p < 0.005$ at a threshold value of 1200).

When scanned at 0.5 mm thickness, 71-mm scan length, 0.8 feed/rotation, and 120 kVp, weighted CT dose indices (CTDIw) were 46.3 mGy for 200 mAs, 59.1 mGy for 250 mAs, and 77.1 mGy for 300 mAs.

Correlation between microstructure parameters and biomechanical properties: To examine whether microstructure parameters correlate with biomechanical properties, another set of four specimens were obtained from the femoral head at surgery and subjected to compression test after scanning by μCT and MDCT. As shown in Fig. 3, microstructure parameters obtained by MDCT revealed a high correlation with ultimate load (kgf); a significant correlation with the ultimate load was obtained for app BV/TV ($p < 0.05$), SMI ($p < 0.05$), and app Th.N ($p < 0.05$).

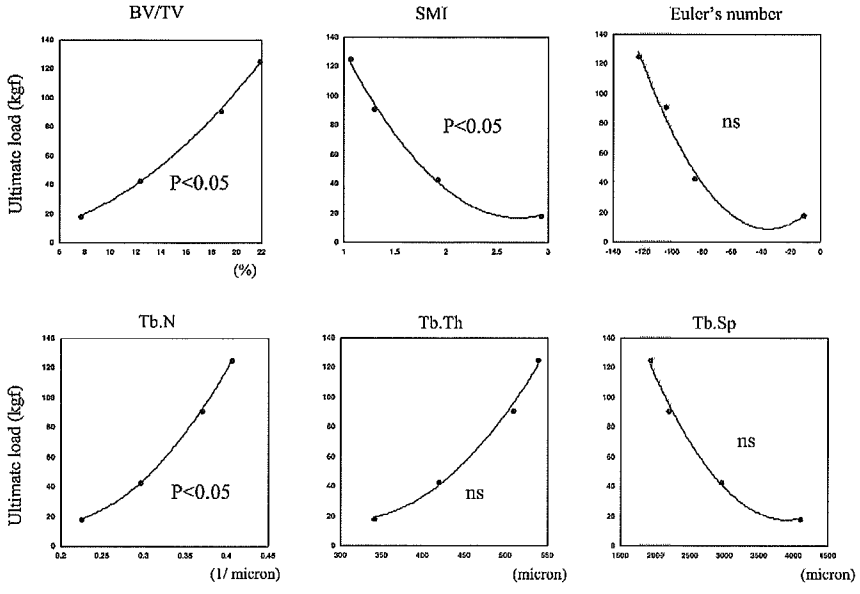

FIG. 3. Correlation between microstructure parameters and bone strength. Ten-millimeter cubic specimens were obtained from the femoral head of four individuals and scanned by μCT and MDCT. Structure analysis was performed as described in the Materials and Methods section. The specimens were subjected to biomechanical test, and the ultimate load was obtained from the load-deformation curve. Shown are significant correlations between microstructure parameters obtained by MDCT and bone strength. p values are shown for each parameter.

Patient study

Association of microstructure parameters with prevalent spinal fracture: To examine the use of trabecular microarchitecture information obtained by MDCT scanning for the assessment of fracture, we compared the microstructure parameters derived from MDCT images between 43 women without fracture (age: 64.4 ± 5.5 years old) and 39 women with a recent spinal fracture (age: 66.2 ± 3.8 years old). As shown in Table 1, there was no significant difference in age, age at menopause, body height (BH), or body weight (BW) between these two groups of women.

Figures 4A–4F show representative 2D (Figs. 4A and 4B), its binarized 2D (Figs. 4C and 4D), and 3D (Figs. 4E and 4F) MDCT images of the third lumbar vertebra of a 62-year-old woman without vertebral fracture (Figs. 4A, 4C, and 4E) and those of a women of the same age with a fracture in the thoracic spine (Figs. 4B, 4D, and 4F).

Table 1 summarizes the results of microstructure parameters, as well as areal (by DXA) and volumetric (by MDCT) BMD values in the two groups of women. Areal BMD by DXA was significantly lower in postmenopausal women with a fracture than in those without one (0.836 ± 0.191 versus 0.925 ± 0.161 g/cm^2, $p < 0.05$). Among the microstructure indices obtained by MDCT, app BV/TV, app Tb.N, app Tb.Th, and fractal dimension were significantly lower; whereas app Tb.Sp, SMI, Euler's number, and DA were significantly higher in women with a fracture than in those without a fracture (Table 1). Volumetric BMD determined by MDCT was also significantly lower in postmenopausal women with a fracture (72.0 ± 18.5 versus 103.9 ± 23.5 mg/cm^3, $p < 0.0001$).

Table 2 shows the correlation of microstructure parameters with BMD values obtained by DXA and QCT. Most microstructure parameters were more highly correlated with volumetric BMD by QCT than with areal BMD by DXA.

ROC analysis was performed to determine the diagnostic value of microstructure parameters with respect to fracture (Table 3). The highest AUC value was obtained for SMI (0.928), which was significantly higher than that for areal BMD by DXA (0.647) or volumetric BMD by MDCT (0.870). AUC values of Euler's number (0.857) and app Tb.Sp (0.818) were similar to that value of volumetric BMD, and significantly exceeded that of areal BMD by DXA. The ORs for the association of SMI (16.0), app BV/TV (13.6), Euler's number (13.1), app Tb.Sp (7.4), fractal dimension (7.4), app Tb.N (6.6), and app Tb.Th (5.5) with fracture were higher than the OR for that of areal BMD by DXA with it (4.8); the ORs for SMI, app BV/TV, and Euler's number exceeded that ratio of volumetric BMD (12.7). Multivariate regression analysis showed significant correlations of SMI (R^2 = 0.329, $p < 0.0001$) and Tb.Th (R^2 = 0.154, $p < 0.005$), as well as volumetric BMD (R^2 = 0.159, $p < 0.005$), with fracture (Table 4). Combining areal or volumetric BMD data with some microstructural parameters further increased R^2 values compared with BMD alone (Table 4).

Table 5 shows the correlations of spinal microarchitecture or BMD with age and BW. Most microstructure parameters and volumetric BMD by MDCT correlated with age, especially SMI, Euler's number, and app BV/TV, whereas areal BMD values by DXA showed a moderate correlation with both age and BW.

DISCUSSION

The purpose of this study was to evaluate the diagnostic value of in vivo analysis of spinal trabecular microstructure, focusing on its association with prevalent spinal fracture. Compared with postmenopausal women without a spinal fracture, those with one had a smaller trabecular bone fraction (app BV/TV: 36.1 versus 26.2) in association with fewer

TABLE 1. COMPARISON OF VERTEBRAL MICROSTRUCTURAL PARAMETERS BETWEEN TWO GROUPS WITHOUT AND WITH FRACTURE

	Without fracture (n = 43)	*With fracture (n = 39)*	*p (by t-test)*
Background data			
Anthropometric data			
Age (years)	64.4 ± 5.5	66.2 ± 3.8	NS
Age at menopause (years)	50.3 ± 2.8	48.9 ± 4.2	NS
Body height (cm)	152.3 ± 4.7	150.1 ± 7.2	NS
Body weight (kg)	52.8 ± 7.3	50.1 ± 7.8	NS
Areal BMD by DXA (g/cm^2)	0.925 ± 0.161	0.836 ± 0.191	0.05
MDCT data			
Microstructure parameters			
App BV/TV (%)	36.1 ± 7.0	26.1 ± 8.5	<0.0001
App Tb.N (1/mm^3)	0.97 ± 0.09	0.78 ± 0.20	<0.0001
App Tb.Th (μm)	368.3 ± 46.1	335.8 ± 46.2	0.005
App Tb.Sp (μm)	667 ± 129	1064 ± 439	<0.0001
Structure model index	1.87 ± 0.48	2.70 ± 0.38	<0.0001
Euler's number	−1037 ± 375	−457 ± 404	<0.0001
Fractal dimension	2.52 ± 0.06	2.41 ± 0.18	0.0005
Degree of anisotropy	1.44 ± 0.15	1.58 ± 0.35	0.05
Volumetric BMD (mg/cm^3)	103.9 ± 23.5	72.0 ± 18.5	<0.0001

Data are shown as mean ± SD.

app BV/TV, apparent bone volume fraction; app Tb.N, apparent trabecular number; app Tb.Th, apparent trabecular thickness; app Tb.Sp, apparent trabecular separation; NS, not significant.

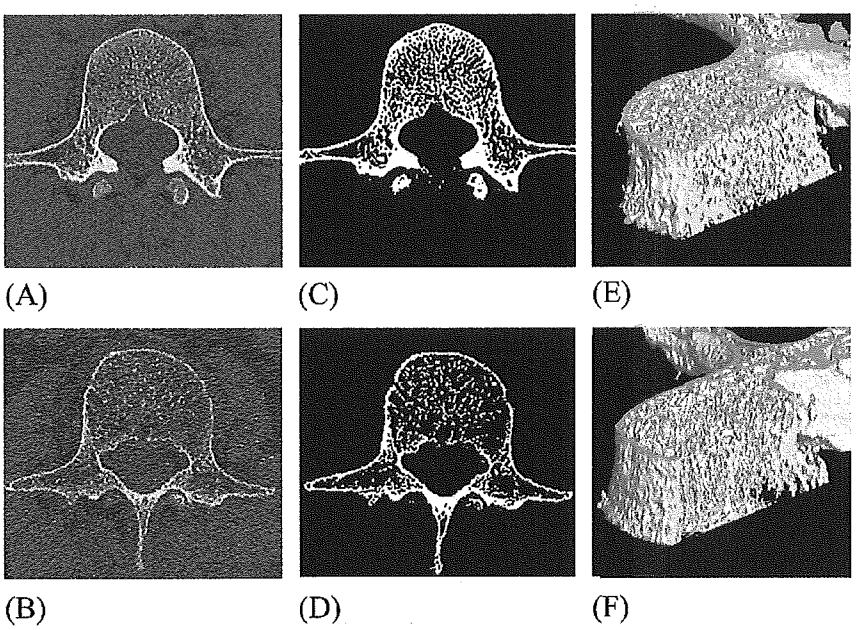

FIG. 4. Representative 2D and 3D MDCT images of the third lumbar spine. (A and B) 2D and (E and F) 3D MDCT images of the third lumbar spine were obtained from (A and E) a 62-year-old woman without vertebral fracture and (B and F) a woman of the same age with a vertebral fracture in her thoracic spine. (C and D) Binarized images are also shown.

trabeculae (app Tb.N: 0.97 versus 0.78), more rodlike structure (SMI: 1.87 versus 2.70), and lower connectivity (Euler's number: −1037 versus −457). The ORs of microstructure parameters, such as SMI, Euler's number, and app BV/TV, for association with prevalent fracture were much higher than that ratio for association of areal BMD by DXA with it. SMI and Euler's number, which represent nonmetric features of trabecular structure, would seem to be more useful than metric parameters such as app Tb.N, app Tb.Th, or app Tb.Sp. It is an advantage of the MDCT scanning system that, in addition to assessing these 3D microstructure parameters, volumetric BMD values can be obtained at the same time by using a reference phantom; these values correlate highly with the presence of fracture.

In vivo analysis of trabecular microstructure has been studied using conventional radiography, high-resolution CT, and high-resolution MRI. Conventional radiography has a spatial resolution of up to 40 μm; however, it delivers projectional images of the trabecular structure. Conventional high-resolution CT with spatial resolution of 400 μm shows only structural texture, because the trabecular structure is subjected to partial-volume effects. With the use of

TABLE 2. CORRELATIONS BETWEEN MICROSTRUCTURAL PARAMETERS AND BMD

Structure parameters by MDCT	*Volumetric BMD by QCT*		*Areal BMD by DXA*	
	R^2	*p*	R^2	*p*
App BV/TV (%)	0.645	0.0001	0.128	0.005
Structure model index	0.514	0.0001	0.151	0.0005
App Tb.Th (μm)	0.487	0.0001	0.083	0.01
Euler's number	0.433	0.0001	0.125	0.005
App Tb.N (1/mm^3)	0.428	0.0001	0.104	0.005
App Tb.Sp (μm)	0.350	0.0001	0.045	NS
Fractal dimension	0.311	0.0001	0.213	0.0001
Degree of anisotropy	0.084	0.01	0.034	NS

app BV/TV, apparent bone volume fraction; app Tb.Th, apparent trabecular thickness; app Tb.N, apparent trabecular number; app Tb.Sp, apparent trabecular separation; NS, not significant.

TABLE 3. ROC ANALYSIS AND ORS OF MICROSTRUCTURAL PARAMETERS FOR THEIR ASSOCIATION WITH SPINAL FRACTURE

Measurements	*AUC (ROC)*	*p*	*OR (95% CI)*	*p*
MDCT				
Microstructural parameters				
Structural model index	0.928 ± 0.027	0.0001	16.0 (5.3–48.4)	0.0001
App BV/TV (%)	0.811 ± 0.048	0.0001	13.6 (4.3–42.4)	0.0001
Euler's number	0.857 ± 0.043	0.0001	13.1 (4.5–38.1)	0.0001
App Tb.Sp (μm)	0.818 ± 0.048	0.0001	7.4 (2.8–19.8)	0.0001
Fractal dimension	0.735 ± 0.059	0.0001	7.4 (2.6–20.7)	0.0005
App Tb.N (1/mm^3)	0.810 ± 0.049	0.0001	6.6 (2.5–17.4)	0.0005
App Tb.Th (μm)	0.674 ± 0.059	0.01	5.5 (1.6–18.5)	0.01
Degree of anisotropy	0.627 ± 0.063	0.05	3.5 (1.2–10.2)	0.05
Volumetric BMD (mg/cm^3)	0.870 ± 0.040	0.0001	12.7 (4.4–36.4)	0.0001
DXA areal BMD (g/cm^2)	0.647 ± 0.062	0.05	4.8 (1.5–14.8)	0.05

Data are shown as mean ± SD.

app BV/TV, apparent bone volume fraction; app Tb.Sp, apparent trabecular separation; app Tb.N, apparent trabecular number; app Tb.Th, apparent trabecular thickness.

TABLE 4. CORRELATION OF MICROSTRUCTURE PARAMETERS AND BMD WITH FRACTURE

vBMD with microstructure parameters			*aBMD with microstructure parameters*		
Measures	R^2	*p*	*Measures*	R^2	*p*
vBMD	0.366	0.0001	aBMD	0.061	0.0251
SMI	0.486	0.0001	SMI	0.486	0.0001
Tb.Th	0.112	0.0021	Euler's number	0.362	0.0001
vBMD + SMI	0.508	0.0001	aBMD + SMI	0.486	0.0001
vBMD + SMI + Tb.T	0.551	0.0001	aBMD + SMI + Euler's number	0.506	0.0001

Correlation with prevalent vertebral fracture was assessed by multivariate regression analysis.

vBMD, volumetric BMD; aBMD, areal BMD.

high-resolution CT in vivo, analysis of trabecular structure such as connectivity from a skeletonized representation of the trabecular network,[4] parameters derived from run-length encoding,[6] and number or area of holes in trabecular structure[15] have been reported. Their images had a slice thickness of 1.5 mm and the FOV was reduced to yield an image matrix with a pixel size of 0.31 mm. A good relationship between texture parameters calculated from high-resolution CT images and biomechanical properties has also been reported.[5] However, this spatial resolution only provides characteristics of trabecular structure, and 2D image has limited reproducibility among follow-up examinations.

With the recent advances in MRI hardware and software, it has become possible to obtain higher resolution MR images of trabecular bone[16–22] with in-plane resolutions as high as 150 μm and slice thicknesses of 280 μm in vivo.[23] MRI has an advantage of nonionization, and trabecular microstructure obtained in vivo by using high-resolution MR has been shown to be useful in predicting prevalent spinal fractures. Structural parameters of the distal radius with a 3D spin-echo sequence (voxel size of 137 × 137 × 500 μm^3) in 36 female patients were reported to provide a better index than the BMD of the distal radius.[24] 3D gradient-echo sequence (voxel size of 156 × 156 × 500 μm^3) could discriminate between groups with and without a recent hip